Appendix A
Platinum Nanostructures Grown by Focused Electron/Ion Beam Induced Deposition

This appendix presents studies of volume per dose, composition, and high resolution transmission electron microscopy performed on Pt deposits grown by focused electron beam and ion beam induced deposition. The results allow us to correlate the properties studied and different conduction mechanisms proposed in the literature.

Without any doubt, the type of deposit most studied in the literature based on FEBID and FIBID techniques is platinum. The secret of its success lies predominantly in the nature of the precursor materials used for this purpose, in most cases organometallics, which are well known in chemical vapor deposition (CVD). Therefore they are easy to adapt to the technology available in a dual beam system.

We consider it very important to know the deposition rate, composition, and microstructure of the deposits in order to understand and justify the different conduction mechanisms proposed in various publications. In previous studies, the resistivity of Pt nanowires grown by FIBID and FEBID differed considerably as a function of the deposition parameters, although, in general, the deposits grown by FIBID showed lower resistivity values [1–5]. Different conduction mechanisms for Pt nanodeposits have been proposed, but a clear overall idea has not been established, mainly due to the important role played by the carbonaceous matrix. The low Pt percentage in the deposits compared to the carbon from the precursor material is the main handicap to metallic conductivity.

A.1 Platinum Nanostructures Grown by FEBID and FIBID

The precursor material used in our study was cyclopentadienyl trimethyl platinum, $(CH_3)_3Pt(C_pCH_3)$, which is solid at room temperature. This precursor was heated to 45°C. Platinum deposits with dimensions 5 μm × 5 μm were grown on a Si substrate doped with boron. The deposition parameters that were kept constant were overlap 0 %, dwell time 1 μs, refresh time 0 s, $P_{base} = 1 \times 10^{-6}$ mbar, $P_{process} = 2 \times 10^{-5}$ mbar for FEBID and for FIBID overlap 0 %, dwell time 0.2 μs, refresh

R. Córdoba Castillo, *Functional Nanostructures Fabricated by Focused Electron/Ion Beam Induced Deposition*, Springer Theses, DOI: 10.1007/978-3-319-02081-5,

time 0 s, $P_{base} = 1 \times 10^{-6}$ mbar, $P_{process} = 2 \times 10^{-5}$ mbar. Other key parameters, such as accelerating voltage and electron/ion beam current, were varied in order to study their effect on the Pt content, volume per dose, and microstructure.

To calculate the volume per dose VD (μm^3/nC) of the square-shaped deposits (5×5 μm, we must know the thickness, obtained from cross sections, and the electron or ion dose. This was calculated for a large number of nanodeposits with different deposition parameters, which are specified below (see Fig. A.1).

The protocol was as follows: Pt deposits were grown by FEBID at several beam acceleration voltages V_e, from 1 to 30 kV, and at each fixed voltage different deposits were grown at currents I_e from 0.4 to 9.5 nA. It was observed that the electron beam current did not have a significant effect on the VD obtained, suggesting an electron-limited regime.

Figure A.2a shows VD as a function of V_e. We can see VD decreases as a function of V_e, as described for Pt deposits grown by FEBID [7, 8]. As already noted, the decline is quite pronounced above 5 kV and flattens out at around 15 kV. VD at 30 kV is one quarter that at 1 kV. This dependence is explained by the decrease in the number of secondary electrons generated in the substrate and reaching the surface of the sample [7–11].

The probability of dissociation of the precursor molecule is a maximum at energies in the range of a few tens of eV. Moreover, the secondary electron distribution generated by the incident electron beam is a maximum in the same energy range, which favors secondary electrons that contribute greatly to the dissociation of the precursor molecule. As the secondary electron yield decreases with increasing incident acceleration voltage, it is obvious that the deposition yield will decrease with increasing V_e.

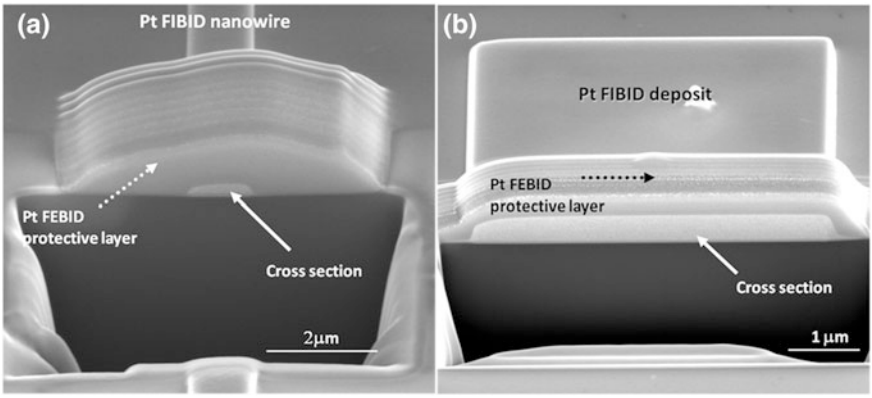

Fig. A.1 SEM images of the cross section of **a** a Pt nanowire grown by FIBID and **b** a square-shaped deposit grown by FIBID. In both cases, in order to protect the area of interest and to obtain good contrast in the image and so to be able to measure the deposit thickness of interest, before the ion milling a Pt layer grown by FEBID was deposited on top of it. Adapted from [6].

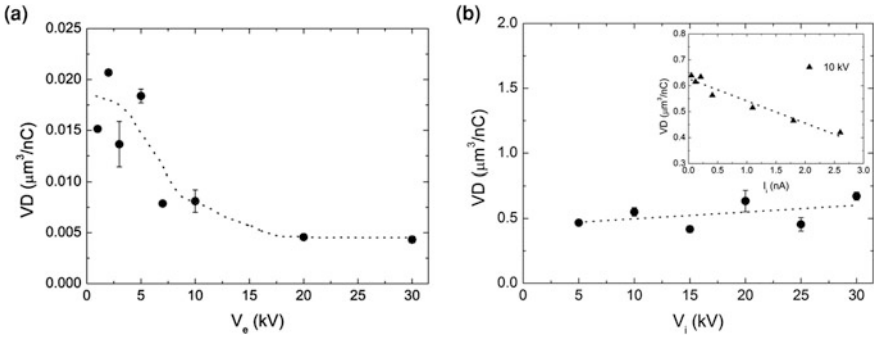

Fig. A.2 **a** Mean and standard deviation (bars) of the VD in Pt deposits grown by FEBID at all beam currents investigated as a function of V_e. **b** Mean and standard deviation of VD in Pt deposits grown by FIBID at all beam currents investigated as a function of V_i. Inset: The deposit VD grown at 10 kV by FIBID as a function of I_i. Adapted from [6].

Pt deposits were grown by FIBID at several V_i ranging from 5 to 30 kV (see Fig. A.2b). At fixed voltage, Pt deposits were grown at different I_i, ranging from 44 pA to 2.6 nA. VD increases slightly as a function of V_i. The Ga^+ FIB interaction depth, even at 30 kV, on silicon is about $\sim$50 nm (SRIM simulations) [12], which allows the generation of a large number of secondary electrons which reach the substrate surface more easily and dissociate the precursor molecules, increasing the VD of FIBID by two orders of magnitude compared to the VD of FEBID. However, we must select the appropriate I_i in order to balance deposition and milling, otherwise we would see effects like that shown in the inset of Fig. A.2b, where VD decreases as a function of I_i.

A.2 Composition and Microstructure of Platinum Nanodeposits

Compositional analysis of the deposits was performed in situ after the deposition process, so deposits were not exposed to environmental conditions, avoiding the possibility that their composition had changed. The thickness of the nanodeposits was around $\sim$160 nm. The V_e used to take the spectra was 10 kV. Figure A.3a presents the Pt content in the deposits grown by FEBID as a function of V_e. It is observed that Pt content decreases from 17 to 11 % as a function of increasing V_e. The C content in the deposit is dominant, at more than 80 %. This decrease in the Pt content is because as V_e increases, the number of secondary electrons (SEs) generated in the substrate and reaching the sample surface that areable to dissociate the precursor gas molecules decreases. However, the interaction of primary beam, the SEs and second-order SEs generated from BSEs electrons make up a complex scenario of the whole process. No significant changes in the deposit content as a function of electron current have been observed. It seems evident that

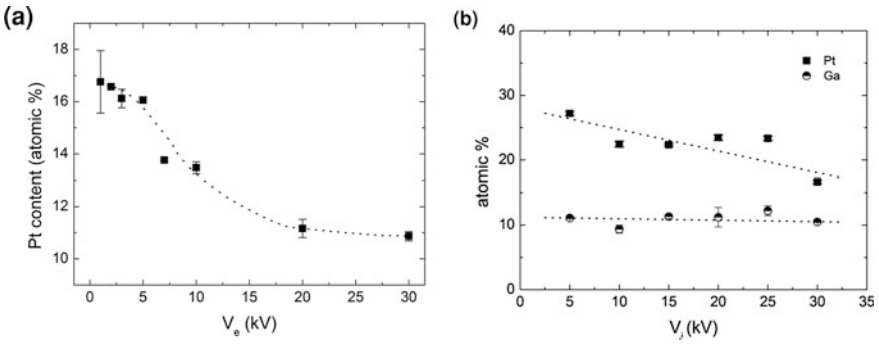

Fig. A.3 **a** Pt content and standard deviation of Pt deposits grown by FEBID at all I_e investigated as a function of V_e. **b** Composition of Pt and Ga (at %) and its standard deviation (bar) in Pt deposits grown by FIBID at all I_i investigated as a function of V_i. Adapted from [6]

the carbonaceous matrix (>80at.% in some cases) will play a crucial role in the conduction mechanism of such deposits.

Figure A.3b presents the Pt and Ga content in the deposits grown by FIBID as a function of V_i. While the Ga content is approximately constant ∼10 %, it is observed that the Pt content decreases from 27 to 17 %. While the C content is still significant, more than 60 %, the metal content (Pt + Ga) is relatively high, which may be responsible for the transport properties manifested by these deposits.

The study of the deposits' microstructure was carried out using HRTEM measurements. The study was performed on Pt deposits grown directly on a commercial Cu grid with a carbon membrane transparent to secondary electrons. Other Pt deposits were studied by inspecting a lamella with thickness below ∼50 nm, after the deposit had been grown on a silicon substrate. In the first approximation, we obtain clear images even though the deposits were grown on

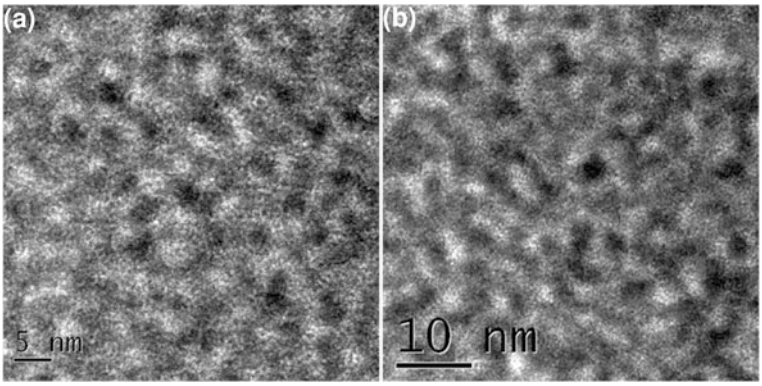

Fig. A.4 HRTEM images of Pt deposits grown at 5 kV by **a** FIBID and **b** FEBID using the dual-beam preparation method. Reprinted from [6]

different substrates. The two studies demonstrate that the two sets of results are compatible.

From EDS results, we know that the main elements of the deposits are C and Pt. However, the interpretation of HRTEM images can be tricky because we obtain two-dimensional images of three-dimensional objects, containing information from the whole thickness of the sample (50 nm). The grains are small compared to the thickness of the sample, and the transmitted electrons can traverse several grains along its path through the sample. The images obtained from the deposits

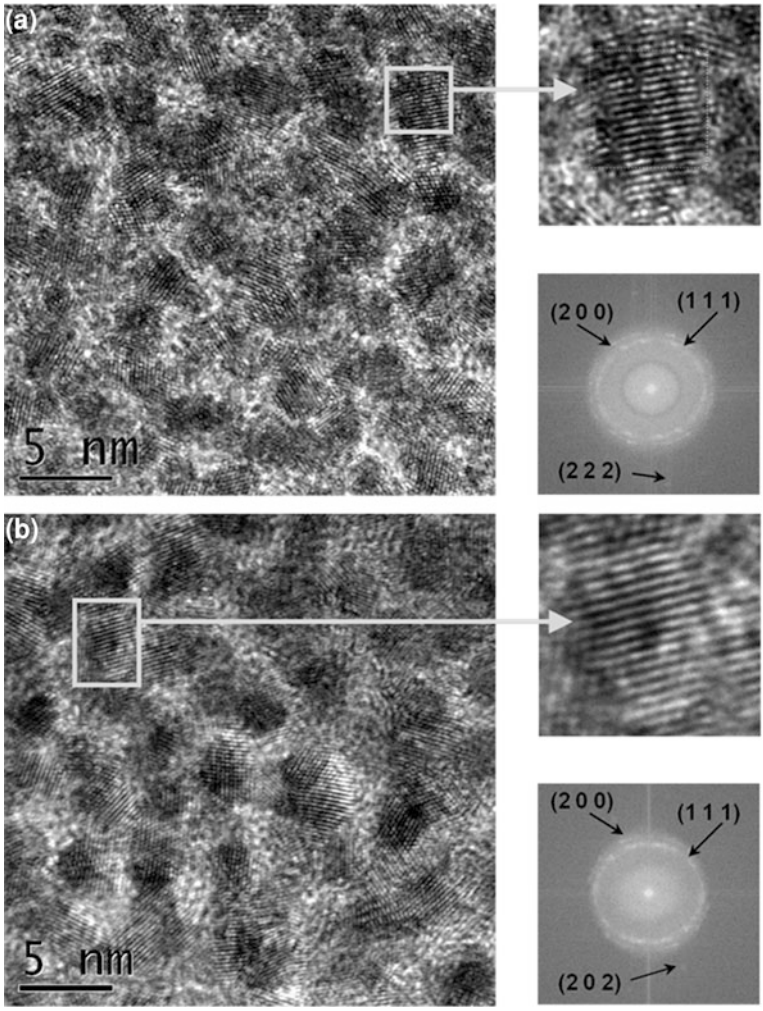

Fig. A.5 HRTEM images of Pt deposits directly grown on a commercial Cu grid at 30 kV by **a** FIBID and **b** FEBID. In each case, one of the grains was selected for clear observation of the corresponding atomic planes. The FFT of the whole image provides the diffraction spots corresponding to the atomic planes of fcc Pt. Adapted from [6]

grown by FEBID and FIBID from the lamellae are shown in Fig. A.4.

The heterogeneous distribution of Pt and C in the microstructure of the deposits has been previously published [1–5] and is explained as Pt nanoparticles with < 5nm size embedded in the amorphous carbon matrix. However, the absence of direct observation of atomic planes is inconvenient for the correct interpretation of the images. Furthermore, the observation of atomic planes in deposits grown directly on Cu grids allows more accurate interpretation of images. As seen in Fig. A.5, Pt deposits grown by FEBID and FIBID consist in ellipsoidal crystalline Pt grains embedded in an amorphous carbon matrix. From FFTs of images, Pt interplanar distances are obtained; the Pt grains have a crystalline face-centered cubic (fcc) structure with lattice parameter 0.3924 nm.

Deposits at different voltages and currents, for both FIBID and FEBID, were studied. After analyzing at least 50 individual grains in each image, we found that the average crystal size of Pt in deposits is 3.2 ± 0.8 nm.

From HRTEM images of Pt deposits grown by FEBID and FIBID, obtained from the lamellae or the deposits grown directly on Cu grids, we see that the microstructure is qualitatively similar. However, for a quantitative analysis only the deposits grown on Cu grids allow us to draw conclusions.

References

1. Langford, R.M., Wang, T.X., Ozkaya, D.: Reducing the resistivity of electron and ion beam assisted deposited Pt. Microelectron. Eng. **84**(5–8), 784–788 (2007)
2. Lin, J.F., Bird, J.P., Rotkina, L., Sergeev, A., Mitin, V.: Large effects due to electron-phonon-impurity interference in the resistivity of Pt/C-Ga composite nanowires. Appl. Phys. Lett. **84**(19), 3828–3830 (2004)
3. Rotkina, L., Lin, J.F., Bird, J.P.: Nonlinear current-voltage characteristics of Pt nanowires and nanowire transistors fabricated by electron-beam deposition. Appl. Phys. Lett. **83**(21), 4426–4428 (2003)
4. Lin, J.F., Bird, J.P., Rotkina, L., Bennett, P.A.: Classical and quantum transport in focused-ion-beam-deposited Pt nanointerconnects. Appl. Phys. Lett. **82**(5), 802–804 (2003)
5. Peñate-Quesada, L., Mitra, J., Dawson, P.: Non-linear electronic transport in Pt nanowires deposited by focused ion beam. Nanotechnology **18**(21), 215203 (2007)
6. De Teresa, J.M., Córdoba, R., Fernández-Pacheco, A., Montero, O., Strichovanec, P., Ibarra, M.R.: Origin of the difference in the resistivity of as-grown focused-ion- and focused-electron-beam-induced Pt nanodeposits. J. Nanomater. **2009**, 936863 (2009). doi:10.1155/2009/936863
7. Lipp, S., Frey, L., Lehrer, C., Demm, E., Pauthner, S., Ryssel, H.: A comparison of focused ion beam and electron beam induced deposition processes. Microelectron. Reliab. **36**(11–12), 1779–1782 (1996)
8. Takai, M., Jarupoonphol, W., Ochiai, C., Yavas, O., Park, Y.K.: Processing of vacuum microelectronic devices by focused ion and electron beams. Appl. Phys. A Mater. Sci. Process. **76**(7), 1007–1012 (2003)
9. Silvis-Cividjian, N., Hagen, C.W., Kruit, P.: Spatial resolution limits in electron-beam-induced deposition. J. Appl. Phys. **98**(8), 084905 (2005)
10. Utke, I., Hoffmann, P., Melngailis, J.: Gas-assisted focused electron beam and ion beam processing and fabrication. J. Vac. Sci. Technol. B **26**(4), 1197–1276 (2008)

11. van Dorp, W.F., Hagen, C.W.: A critical literature review of focused electron beam induced deposition. J. Appl. Phys. **104**(8), 081301 (2008)
12. Ziegler, J.F.: SRIM-2003. Nucl. Instrum. Methods Phys. Res., Sect. B **219–220**, 1027–1036 (2004)